

1 ! " # \$ % & ' () * * +, - .) + " (+ / (*), 0 & 1 (" \$ " + 2 \$ 1.) % & * () " (\$ (2 # 3 *) % \$, (
2 4) 5. - 1 & (6). # (2, \$.) " - 4 (" \$ " + 2 \$ 1.) % & * (7 \$ * & ' (+ " (. # & (
3 * \$ % a /)) % a \$, (\$ " + ' & (& / & % (
4

5 Marina Breisch[!], Kateryna Loza[#], Kevin Pappert[#], Alexander Rostek[#], Christian
6 Rurainsky^{\$}, Kristina Tschulik^{\$}, Marc Heggen[%], Matthias Epple[#], Jörg C. Tiller[&],
7 Thomas A. Schildhauer[!], Manfred Köller[!], Christina Sengstock[!]

8
9 [!] BG University Hospital Bergmannsheil Bochum / Surgical Research, Ruhr
10 University Bochum, Buerkle-de-la-Camp-Platz 1, D-44789 Bochum, Germany. Fax:
11 +49 234 3024734; Tel: +49 234 3024724; E-mail: marina.breisch@tu-dortmund.de

12 [#] University of Duisburg-Essen, Inorganic Chemistry and Center for Nanointegration
13 Duisburg-Essen (CeNIDE), Universitaetsstr. 5-7, D-45117 Essen, Germany.

14 ^{\$} Ruhr University Bochum, Faculty of Chemistry and Biochemistry, Electrochemistry
15 and Nanoscale Materials, Universitätsstr. 150, D-44780 Bochum, Germany.

16 [%]Ernst Ruska-Centre (ER-C) for Microscopy and Spectroscopy with Electrons,
17 Research Center Jülich GmbH, 52425 Jülich, Germany.

18 [&] TU Dortmund University, Faculty of Biochemical and Chemical Engineering,
19 Institute for Biomaterials and Polymer Science, Emil-Figge-Straße 50, 44227
20 Dortmund, Germany.

21
22 * Corresponding author, Tel: +49 234 3024724, Fax: +49 234 3024734, e-mail:
23 marina.breisch@tu-dortmund.de

1 ! " # \$ % & ' () * + , - . : ;

2

3 A strategy to reduce implant-related infections is the inhibition of the initial bacterial
4 implant colonization by biomaterials containing silver (Ag). The antimicrobial efficacy
5 of such biomaterials can be increased by surface enhancement (nanosilver) or by
6 creating a sacrificial anode system for Ag. Such a system will lead to an
7 electrochemically driven enhanced Ag ion release due to the presence of a more
8 noble metal. Here we combined the enlarged surface of nanoparticles (NP) with a
9 possible sacrificial anode effect for Ag induced by the presence of the
10 electrochemically more noble platinum (Pt) in physical mixtures of Ag NP and Pt NP
11 dispersions.

12 These Ag NP / Pt NP mixtures were compared to same amounts of pure Ag NP in
13 terms of cell biological responses, i.e. the antimicrobial activity against
14 ! " # \$ % & ' () * + , - . : ; as well as the viability of human
15 mesenchymal stem cells (hMSC). In addition, Ag NP was analyzed by ultraviolet-
16 visible (UV-Vis) spectroscopy, cyclic voltammetry (CV), and atomic absorption
17 spectroscopy (AAS).

18 It was found that the dissolution rate of Ag NP was enhanced in the presence of Pt
19 NP within the physical mixture compared to a dispersion of pure Ag NP. Dissolution
20 experiments revealed a fourfold increased Ag ion release from physical mixtures due
21 to enhanced electrochemical activity, which resulted in a significantly increased
22 toxicity towards both bacteria and hMSC. Thus, our results provide evidence for an
23 underlying sacrificial anode mechanism induced by the presence of Pt NP within
24 physical mixtures with Ag NP. Such physical mixtures have a high potential for
25 various applications, for example as antimicrobial implant coatings in the biomedicine
26 or as bactericidal systems for water and surface purification in the technical area.

27

28 **Keywords:** sacrificial anode, antimicrobial activity, silver nanoparticles, platinum
29 nanoparticles, physical mixture

30

1)*(+ \$%. / ' \$D , (

2

3 Despite best clinical practice, implant-related infections remain a serious clinical
4 problem [1]. Antimicrobially active biomaterials or coatings containing silver (Ag)
5 which could prevent or hinder the initial bacterial adhesion, colonization and biofilm
6 formation are promising approaches to reduce implant-related infections.

7 Numerous studies demonstrated the capability of Ag to reduce infections and
8 bacterial colonization of burn dressings, catheters, dental implants and other medical
9 devices [2–6]. It is now generally accepted that the biological action of Ag is based
10 on the oxidative release of silver ions (Ag⁺) which interact with various biomolecules
11 such as enzymes, nucleic acids and cell wall components [7–10]. Thus, the
12 antibacterial activity of Ag is governed by the amount of released Ag⁺. In general, the
13 increased surface area of Ag nanoparticles (NP) compared to macroscale Ag leads
14 to a more efficient Ag⁺ release [11].

15 In previous studies we investigated an alternative approach to enhance the Ag⁺
16 release by the combination of Ag with an electrochemically more noble metal, i.e. a
17 platinum group element, based on the sacrificial anode principle [12–14]. Generally,
18 when two electrochemically different metals are present in an electrolytic
19 environment, an anodic polarization is induced, and the less noble metal is dissolved
20 ("sacrificed") in favor of the more noble one by corrosion [15]. Sacrificial anodes are
21 widespread in the technical area [15–17], but have not received much attention in
22 biomedical applications so far.

23 There are only few studies that have addressed the biological effects of Ag-related
24 sacrificial anode-like systems. j hang . ", #'1 found that bimetallic nanosheets of Ag
25 (7 nm) and platinum (Pt; 1 – 3 nm) on porous reduced graphene oxide showed
26 increased antimicrobial activity against / +) % -0 % #,) ('0 due to an enhanced Ag⁺
27 release compared to pure Ag sheets [18]. Dowling . ", #'1 demonstrated an improved
28 antibacterial efficiency of alloyed bimetallic AgPt coatings on polymeric surfaces
29 compared to pure Ag coatings [19]. k ur group showed the efficiency of sacrificial
30 anode systems consisting of Ag dots deposited on thin metal films of gold, platinum,
31 palladium or iridium [12–14].

32 Recently, we investigated whether an enhanced Ag⁺ release based on the sacrificial
33 anode principle could be achieved by combination of Ag with the electrochemically
34 more noble Pt in the form of NP. I e found that no sacrificial anode effect was

1 induced in bimetallic alloyed AgPt NP [20,21]. Therefore, we investigated mixtures of
2 non-alloyed Ag NP and Pt NP (physical mixture in aqueous dispersion) in comparison
3 to pure Ag NP. To identify a possible sacrificial anode effect (enhanced Ag⁺ release)
4 induced by the physical mixture, we analyzed the antimicrobial activity towards gram-
5 positive *Staphylococcus aureus* (ATCC 29213) and gram-negative *Escherichia coli* (ATCC 8739) as well as the viability of human mesenchymal stem cells (hMSC). In
6 addition, ultraviolet–visible (UV-Vis) spectroscopy, cyclic voltammetry (CV), and
7 atomic absorption spectroscopy (AAS) were performed to assess the Ag NP
8 dissolution.

10
11
12 1.2. Synthesis and characterization of Ag and Pt NPs

14 2.1. Synthesis of Ag and Pt NPs

15 Pure Ag NP and pure Pt NP were synthesized as reported earlier [22] by reducing
16 silver nitrate (AgNO₃; 99.90%, Carl Roth, Karlsruhe, Germany) or hexachloroplatinic
17 acid (H₂PtCl₆; 99.90%, Carl Roth) with sodium borohydride (NaBH₄; 96%, Sigma-
18 Aldrich, Taufkirchen, Germany) or citrate/tannic acid (anhydrous 98%, Acros
19 2-3405, Nidderau, Germany / Fluka, Munich, Germany). The NP were coated
20 with poly(N-vinylpyrrolidone) (PVP, Povidon 30, M_w 40,000 g mol⁻¹, Fluka), and the
21 average NP diameter was about 7 nm for both NP species, as was analyzed by
22 differential centrifugal sedimentation (DCS) and high resolution transmission electron
23 microscopy (HR-TEM) [22]. For full characterization data of Ag NP and Pt NP see
24 Rostek et al., 2018 [22].

25 The synthesized NP were stored in degassed ultrapure water under argon until
26 further analysis or application. Stock solutions of NP were prepared in sterile
27 ultrapure water (1.0, 0.7, 0.5, 0.2, 0.1 mg mL⁻¹). To achieve the final metal
28 concentrations of 50, 35, 25, 10 and 5 µg mL⁻¹ of each dispersion 50 µL were added
29 per 1 mL of sample. Physical mixtures of Ag NP and Pt NP were prepared by simply
30 mixing of the two monometallic NP dispersions.

31 Solutions of silver acetate (AgAc; ReagentPlus 99%, Sigma-Aldrich) used as Ag⁺
32 control were prepared in sterile ultrapure water and normalized to the total content
33 of Ag.

1 **2.2** , - * (2, (. (34\$

2 / +) % - 0 % # ,) (' 0 DH5a (/ 1) (' 0 German Collection of Microorganisms and Cell
3 Cultures (DSMj) 6897) and ! "# \$ % & () () * + , # * - . * + (! 1 , # * - . * + ; DSMj 1104) were
4 cultured overnight in RPMI1640 (RPMI; GIBcK , Invitrogen, Karlsruhe, Germany)
5 containing 10o (v/v) fetal calf serum (FCS; GIBcK , Invitrogen) and L-glutamine
6 (0.3 g L⁺¹; GIBcK , Invitrogen) at 37 sC using a shaking water bath. Bacterial cell
7 number was measured using a Densichek turbidity photometer (bioMerieux, Lyon,
8 France), based on turbidity standard solutions (McFarland scale).

9 The antimicrobial activity of NP was analyzed by determination of the minimum
10 inhibitory concentration (MIC, lowest NP concentration able to inhibit bacterial
11 growth) and the minimum bactericidal concentration (MBC, lowest NP concentration
12 that kills 99.9o of the bacteria). Bacterial cell cultures were prepared by dilution of
13 overnight cultures in RPMI/FCS. After addition of the different NP (35, 25, 10,
14 5 r g mL⁺¹), bacterial suspensions (10[&], 10[%], 10^{\$} colony forming units (CFU) mL⁺¹)
15 were incubated for 24 h under cell culture conditions. Subsequently, the MIC was
16 determined by visual assessment of the sample turbidity. The MBC was determined
17 by plating of 50 r L of the samples without visible turbidity on Columbia agar plates
18 (bioMerieux) and examination of the formed bacterial colonies after 24 h incubation at
19 37 sC in a microbial incubator.

20

21 **2.5** \$ / .. \$ 7 . + 7 * / \$

22 Human mesenchymal stem cells (hMSC; 5[·] to 10[·] passage, Lonza, Basel,
23 Switzerland) were cultivated in cell culture medium RPMI/FCS using 75 cm[#] culture
24 flasks (BD Falcon, Becton Dickinson GmbH, Heidelberg, Germany). Cells were
25 grown at 37 sC in a humidified 5o Ck # atmosphere and sub-cultivated every 7 d to
26 14 d depending on cell proliferation.

27 Adherent subconfluent growing hMSC were detached from the culture flasks after
28 washing with phosphate-buffered saline solution (PBS; GIBcK , Invitrogen) by
29 addition of 0.2 mL cm^{+#} 0.25o trypsin/0.05o ethylenediaminetetraacetic acid (v/v)
30 (EDTA, Sigma-Aldrich) for 5 min at 37 sC. Subsequently, cells were harvested,
31 washed twice with RPMI/FCS and seeded at a density of 1.5 x 10[%] cells per well in
32 24-well cell culture plates (BD Falcon).

33

34 **2.8** \$ / .. \$ 9 , & 2 , , + 4 \$

1 Adherent hMSC were treated either with dispersions of pure Ag NP, pure Pt NP or a
2 physical mixture of Ag NP and Pt NP for 24 h in RPMI/FCS under cell culture
3 conditions.

4 After NP exposure, cells were stained with 1 μ M calcein-acetoxymethylester (calcein-
5 AM; Calbiochem, Schwalbach, Germany) for 30 min at 37 $^{\circ}$ C and 50 μ g mL $^{-1}$
6 propidium iodide (PI; Sigma-Aldrich) for 10 min at RT (Live-Dead staining).
7 Subsequently, the stained cells were analyzed by fluorescence microscopy (klympus
8 MVu10, klympus, Hamburg, Germany). Cell viability was quantified by phase
9 analysis (CellSens Dimensions, klympus) calculating the calcein-fluorescent area.
10 The data of NP treated hMSC was given as percentage of the non-treated control
11 area, which was set as 100%.

12 Time-lapse microscopy was performed using the CytoSMART system (Lonza).
13 Adherent hMSC were exposed to pure Ag NP (35 μ g mL $^{-1}$), a physical mixture of Ag
14 NP with Pt NP (35 μ g mL $^{-1}$ of each NP) or an AgAc solution (3.5 μ g mL $^{-1}$ Ag; Sigma-
15 Aldrich) in RPMI/FCS under cell culture conditions and images of the cell culture
16 were taken every 30 min.

17

18 **2.1. UV-Vis absorption spectra**

19 UV-Vis absorption spectra were recorded at room temperature using the UV-Vis
20 spectrophotometer UVmini-1240 (Shimadzu, Kyoto, Japan) with semi-micro UV-
21 cuvettes (Brandt GmbH, Lärtheim, Germany).

22 Pure Ag NP (50 μ g mL $^{-1}$) or a physical mixture of Ag NP with Pt NP (50 μ g mL $^{-1}$ of
23 each NP) were dispersed in 1 mL cell culture medium RPMI. Absorption spectra
24 between 300 nm and 500 nm were recorded directly after mixing of the NP (0 min) as
25 well as after 5 min and 15 min incubation of the mixture at room temperature.

26

27 **2.2. Cyclic voltammetry (CV) measurements**

28 For cyclic voltammetry (CV) measurements, a custom-made glassy carbon (GC)
29 electrode (4 mm diameter) was used as the working electrode (WE). An Ag/AgCl,
30 (3 M KCl (aq)) electrode was used as the reference electrode (RE; E $_{0}$ 207 mV vs.
31 standard hydrogen electrode (SHE); SI analytics GmbH, Mainz, Germany). All
32 potentials are given against this reference potential. A graphite rod (6 mm diameter)
33 was used as counter electrode (CE). Before each experiment, the WE was polished
34 to a mirror finish with 1 μ m, 0.3 μ m and 0.05 μ m Al $_2$ O $_3$ particle suspensions (LECK

1 Instruments GmbH). Afterwards, the GC electrode was cleaned by ultra-sonication
2 for 3 min (Elmasonic S 100H, Singen, Germany).

3 NP dispersions of 1 mg mL⁻¹ were then drop-cast onto the I E and dried in an argon
4 flow. Pure Ag NP were applied as a single 2 r L drop. To achieve a physical mixture,
5 Ag NP and Pt NP were simultaneously co-dropped (2 r L of each NP) on the I E. CV
6 measurements were performed in a 0.1 M HCl (am) solution with a scan rate of
7 100 mV s⁻¹ between -0.2 V and 1.25 V. All measurements were carried out with an
8 AutoLab PGStat-12 potentiostat (Metrohm, Herisan, Switzerland).

9

10 2.2.1. Preparation of Ag and Pt NPs

11 Pure Ag NP (50 r g mL⁻¹) or a physical mixture of Ag NP with Pt NP (50 r g mL⁻¹ of
12 each NP) were incubated in 5 mL RPMI in the upper part of an Amicon Ultra-15
13 centrifugal filter (MI Ck q 3,000 Da; Merck Chemicals GmbH, Darmstadt, Germany).
14 After 60 min, 120 min and 180 min of incubation, the NP were separated from the
15 released ions by centrifugation at 4,000 rpm for 60 min.

16 The remaining filtrate (500 r L) was subseuently mixed with 100 r L of concentrated
17 nitric acid for Ag oxidation, and the Ag content was determined by atomic absorption
18 spectrometry (AAS). AAS was carried out with a Thermo Electron M-Series
19 instrument (Thermo Fisher Scientific, I altham, USA) according to DIN EN ISk /IEC
20 17025:2005.

21

22 2.2.2. Data analysis

23 Data are expressed as mean w standard deviation (SD) of at least three independent
24 experiments. Statistical evaluation was performed by one-way analysis of variance
25 (ANk VA) with Holm-Sidak-Test using SigmaPlot Software (Systat Software, Inc., CA,
26 USA). p-Values less than 0.05 were considered as statistically significant.

27

28

29 6*(7 3#/ 4#(

30

31 The postulated sacrificial anode effect and the resulting faster Ag⁺ release from Ag
32 NP induced by the presence of Pt NP was investigated by analysis of antimicrobial
33 activity and cell viability as well as by UV-Vis, CV and AAS measurements of the
34 physical mixture in comparison to a dispersion of pure Ag NP.

1 Three different physical mixtures were prepared containing 30 wto Ag NP / 70 wto
2 Pt NP (Ag30/Pt70), 50 wto Ag NP / 50 wto Pt NP (Ag50/Pt50) and 70 wto Ag NP /
3 30 wto Pt NP (Ag70/Pt30). For comparison of the effects of pure Ag NP and the
4 individual physical mixtures, the respective Ag NP concentration was kept constant,
5 while the Pt NP concentration was varied.

6

7 5.1. Antimicrobial effects of physical mixtures containing Ag NP and Pt NP towards

8 Antimicrobial effects of physical mixtures containing Ag NP and Pt NP towards
9 *Staphylococcus aureus* and *Pseudomonas aeruginosa* were analyzed in comparison to pure Ag NP and pure Pt NP.
10 The Tables 1 and 2 summarize the resulting MBC values for *Staphylococcus aureus* and *Pseudomonas aeruginosa*
11 respectively.

12 Pure Pt NP showed no antimicrobial activity against *Staphylococcus aureus* and *Pseudomonas aeruginosa* even at the
13 highest tested NP concentration of 35 mg mL⁻¹. In contrast, pure Ag NP exhibited
14 significant antimicrobial effects on both strains. The antimicrobial activity of the
15 physical mixtures Ag30/Pt70 and Ag50/Pt50 against *Staphylococcus aureus* and *Pseudomonas aeruginosa* was
16 increased considerably compared to pure Ag NP, which is reflected by a decrease of
17 the MBC values. However, the toxicity of the Ag70/Pt30 mixture was comparable to
18 that of the pure Ag NP.

19 An inoculum effect (IE), which describes the decline of efficacy of antimicrobial
20 agents at increasing bacterial cell number [23,24], was observed for pure Ag NP as
21 well as for all physical mixtures and resulted in an increase of the MBC values for
22 both strains (Tables 1 and 2). However, the overall toxicity ranking was not affected.

23

24

1 **Table 1: MBC of pure Pt 9P: pure ; < 9P and the respective physical B @tures**
 2 **towards ; 7*/70: epressed @ D< BE!" of 9PF** For physical mixtures, the NP
 3 concentration refers to the Ag NP concentration. (n) indicates no bactericidal effect
 4 up to the given concentration, and (p) indicates a bactericidal (MBC) effect at the
 5 given concentration and above.

; 7*/70\$	10 ⁸ CFU mL ^{*!}	10%CFU mL ^{*!}	10 ⁵ CFU mL ^{*!} ,
Pt 9P MBC / r g mL^{*!}	n 35	n 35	n 35
; < 9P MBC / r g mL^{*!}	n 35	p 10 - 25	p 10
; <GHPtJH MBC / r g mL^{*!} Ag NP	p 10 - 25	p 10	p 5
; <KHPtKH MBC / r g mL^{*!} Ag NP	p 10 - 25	p 10	p 5
; <JHPtGH MBC / r g mL^{*!} Ag NP	p 25 - 35	p 10	p 10

6
 7 **Table L: MBC of pure Pt 9P: pure ; < 9P and the respective physical B @tures**
 8 **towards C.\$ (., \$** epressed @ D< BE!" of 9PF For physical mixtures, the NP
 9 concentration refers to the Ag NP concentration. (n) indicates no bactericidal effect
 10 up to the given concentration and (p) indicates a bactericidal (MBC) effect at the
 11 given concentration and above.

C.\$ (., \$	10 ⁸ CFU mL ^{*!}	10%CFU mL ^{*!}	10 ⁵ CFU mL ^{*!} ,
Pt 9P MBC / r g mL^{*!}	n 35	n 35	n 35
; < 9P MBC / r g mL^{*!}	p 35	p 10 - 25	p 5
; <GHPtJH MBC / r g mL^{*!} Ag NP	p 10 - 25	p 5 - 10	p 5
; <KHPtKH MBC / r g mL^{*!} Ag NP	p 25 - 35	p 10	p 5
; <JHPtGH MBC / r g mL^{*!} Ag NP	p 35	p 10 - 25	p 5

12

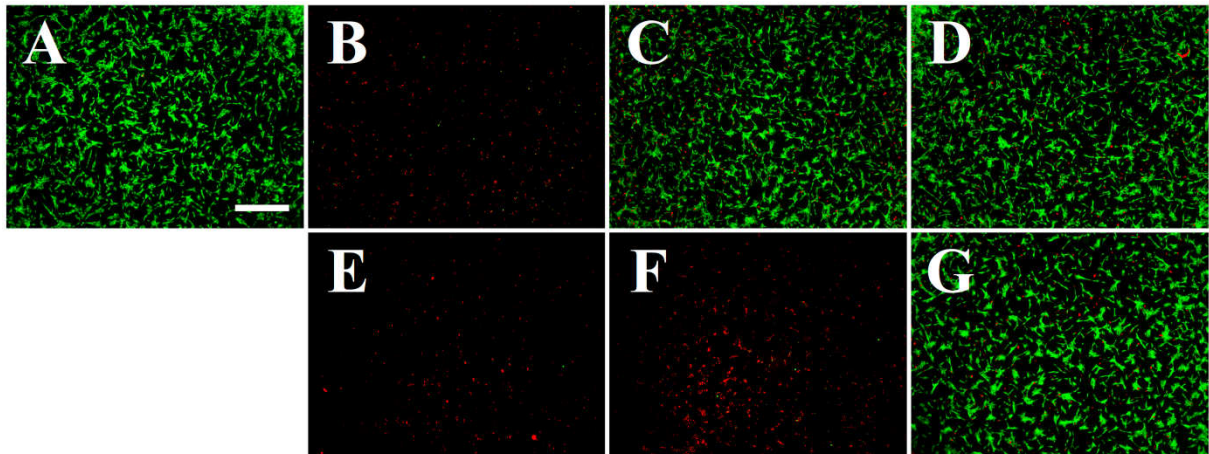
1 5.2\$ / ..\$,&2,,+4\$

2 As was previously reported, released Ag⁽ exert cytotoxic effects on prokaryotic and
3 eukaryotic cells at comparable concentrations [25]. Therefore, the influence of pure
4 Ag NP, pure Pt NP and the respective physical mixtures on the viability of hMSC was
5 analyzed by live-dead staining (Figure 1).

6 Pure Ag NP exhibited significant cell-toxic effects at a concentration of 25 r g mL^{*1} in
7 comparison to the control (untreated hMSC) (Figure 1A - B), whereas Ag NP
8 concentrations below 25 r g mL^{*1} had no adverse effect on cell viability
9 (Figure 1C - D). By contrast, for the physical mixture Ag50/Pt50 cell toxicity was
10 observed already at 10 r g mL^{*1} of Ag NP (Figure 1E - G).

11 The muanitification of cell viability is summarized in Figure 2. Pure Ag NP led to a
12 significant cell toxicity at Ag concentrations of 35 r g mL^{*1} and 25 r g mL^{*1}, while at
13 10 r g mL^{*1} no detectable cell toxicity occurred. Compared to pure Ag NP, the
14 physical mixtures Ag30/Pt70 and Ag50/Pt50 led to significant cell toxic effects
15 already at 10 r g mL^{*1} of Ag NP. In agreement with the antimicrobial activity results
16 (section 3.1) a Pt NP content of 30 wto in the physical mixture did not lead to higher
17 toxicity in comparison to pure Ag NP. After 24 h of exposure no cell toxicity was
18 observed for pure Pt NP up to an NP concentration of 35 r g mL^{*1}.

19

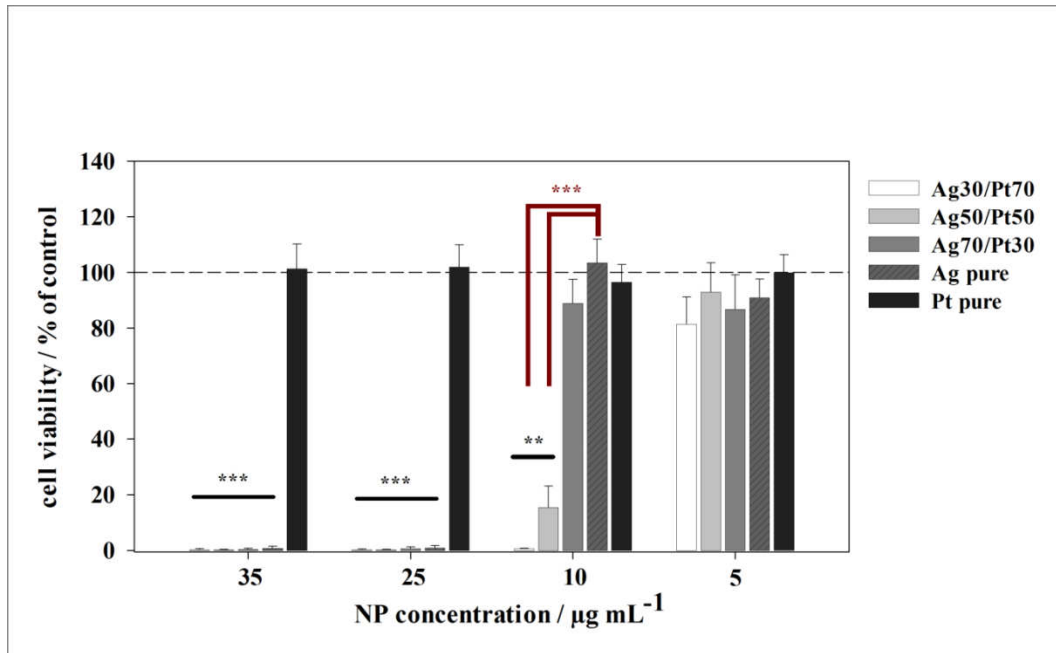


20

21 **Figure 1: Cell morphology of hMSC after 24h exposure.** Representative fluorescence
22 images of hMSC incubated for 24 h with different NP in RMPI/FCS. Cells were
23 stained with calcein-AM (green fluorescence) and PI (red fluorescence) to visualize
24 the morphology of live and dead cells, respectively. ; : hMSC control (no NP
25 exposure). hMSC treated with pure Ag NP (**B**: 25 r g mL^{*1}, **C**: 10 r g mL^{*1}, **O**:

1 5 r g mL⁻¹) or the Ag50/Pt50 physical NP mixture (P: 25 r g mL⁻¹ each, M: 10 r g mL⁻¹,
 2 Q: 5 r g mL⁻¹ of each NP). Scale bar q 2000 r m.

3



4

5 **Figure 3: Cytotoxicity of Ag NPs on hMSC after 24 h exposure.** hMSC were
 6 incubated for 24 h with different NP in RPMI/FCS. Cell viability was determined by
 7 phase analysis of the calcein-AM staining. For physical mixtures, the NP
 8 concentration refers to the Ag NP concentration. Data are expressed as mean \pm SD
 9 of at least three independent experiments and given as the percentage of control (no
 10 NP exposure). Asterisks indicate significant differences ($p < 0.01$, $p < 0.001$) in
 11 comparison to the control (black) or between pure Ag NP and the physical
 12 mixtures (red).

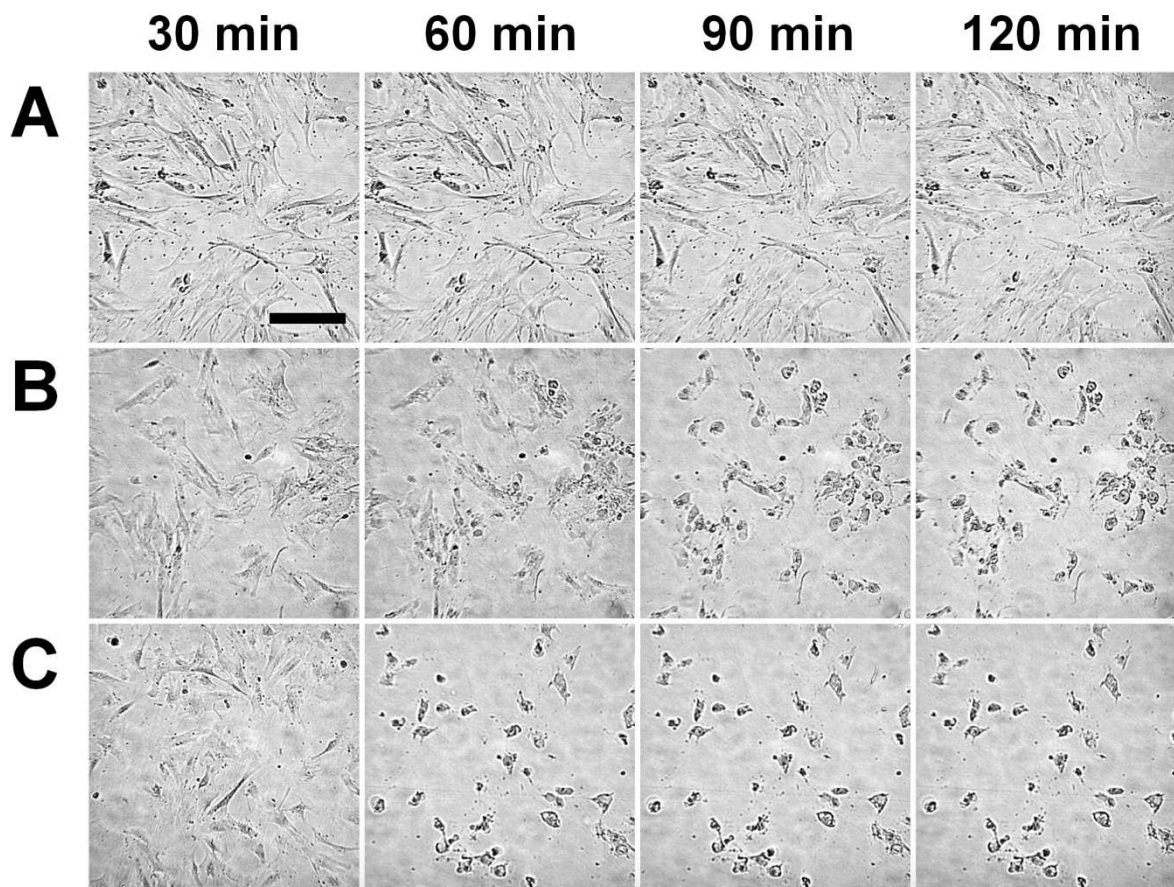
13

14 Time-lapse microscopy was used to elucidate whether the cell-toxic effects occurred
 15 faster with the physical mixtures than with pure Ag NP. Therefore, adherent hMSC
 16 were exposed to pure Ag NP, the physical mixture Ag50/Pt50 or an AgAc solution
 17 (Ag⁺ control) in RPMI/FCS and images of the cell culture morphology were taken
 18 every 30 min.

19 As is shown in Figure 3 (row A), cells incubated with 35 r g mL⁻¹ of pure Ag NP for 2 h
 20 were plastic-adherent and showed a typical fibroblast-like morphology similar to
 21 untreated hMSC. Hence, pure Ag NP induced no visible cell toxicity after 2 h of
 22 incubation. For the physical mixture Ag50/Pt50 containing the same concentration of
 23 Ag NP, toxic effects were observed already after 60 min of incubation, which was

1 visible by morphological changes of the cells (cells became spherical and detached
 2 from cell culture bottom; Figure 3, row B). After 90 min of incubation in the presence
 3 of the physical mixture, all cells had detached. Thus, the presence of Pt NP in the
 4 physical mixture with Ag NP caused a very fast cell death, comparable to the effect of
 5 the AgAc solution (solution of Ag⁺) which led to complete cell detachment within
 6 60 min of incubation (Figure 3, row C).

7



8

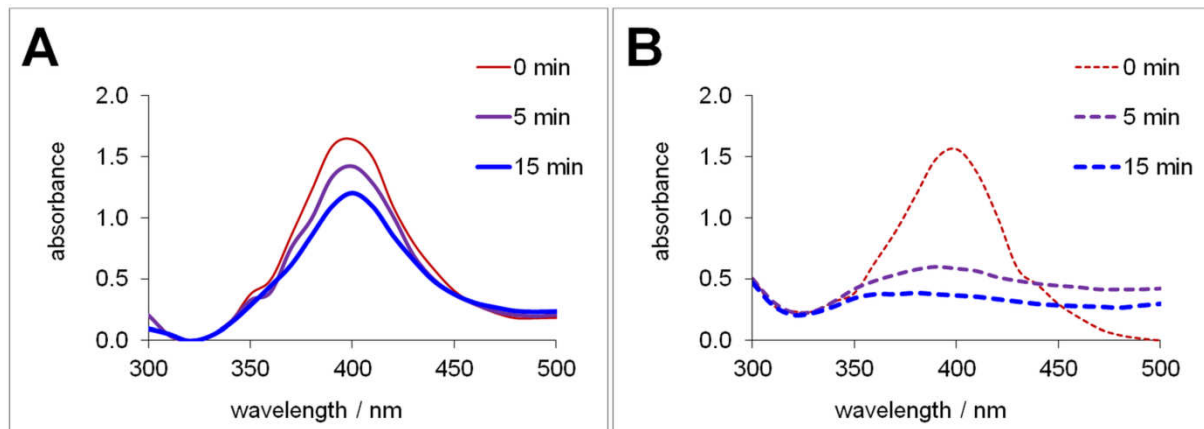
9 **Figure 3. Time-lapse microscopy of hMSC during exposure.** Representative
 10 time-lapse images of hMSC incubated with pure Ag NP ($35 \text{ } \mu\text{g mL}^{-1}$, **row A**), the
 11 Ag50/Pt50 physical mixture ($35 \text{ } \mu\text{g mL}^{-1}$ of each NP, **row B**), and an AgAc solution
 12 ($3.5 \text{ } \mu\text{g mL}^{-1}$ Ag, **row C**). Living cells are plastic-adherent with a typical fibroblast-like
 13 morphology. Dead cells can be recognized by changed morphology (spherical,
 14 detaching cells). Scale bar = 200 μm .

15

16 5.5×10^{-4} (0.00055) $\times 40,000$

17 Dispersions of Ag NP exhibit a characteristic optical absorption spectrum due to
 18 surface plasmon resonance (SPR) which correlates with the particle morphology [26–

1 29]. Spherical and approximately spherical Ag NP display a single absorption
 2 maximum between 390 nm and 460 nm, depending on the particle size [26,30,31].
 3 Therefore, changes in peak height, area and position can be used to monitor an
 4 altered particle size, shape or surface, e.g. by NP dissolution.
 5 To track the time-dependent change of the Ag NP absorption spectra, pure Ag NP or
 6 the physical mixture Ag50/Pt50 were dispersed in RPMI and the spectra were
 7 measured between 300 nm and 500 nm. As is shown in Figure 4A, the Ag NP used
 8 in this study (spherical, diameter about 7 nm) displayed one single absorption
 9 maximum at 400 nm. Pure Pt NP does not have an absorption maximum in this
 10 wavelength range [32]. The height of the absorption peak of pure Ag NP decreased
 11 slightly during 15 min of incubation in RPMI, indicating a minor NP transformation
 12 (Figure 4A). In contrast, in the case of the physical mixture the plasmon Ag peak
 13 declined rapidly after 5 min of incubation in RPMI and disappeared completely
 14 already after 15 min of incubation in RPMI (Figure 4B). The fast and strong decline of
 15 the Ag NP absorption peak in the physical mixture suggests that a substantial Ag NP
 16 alteration has taken place.
 17

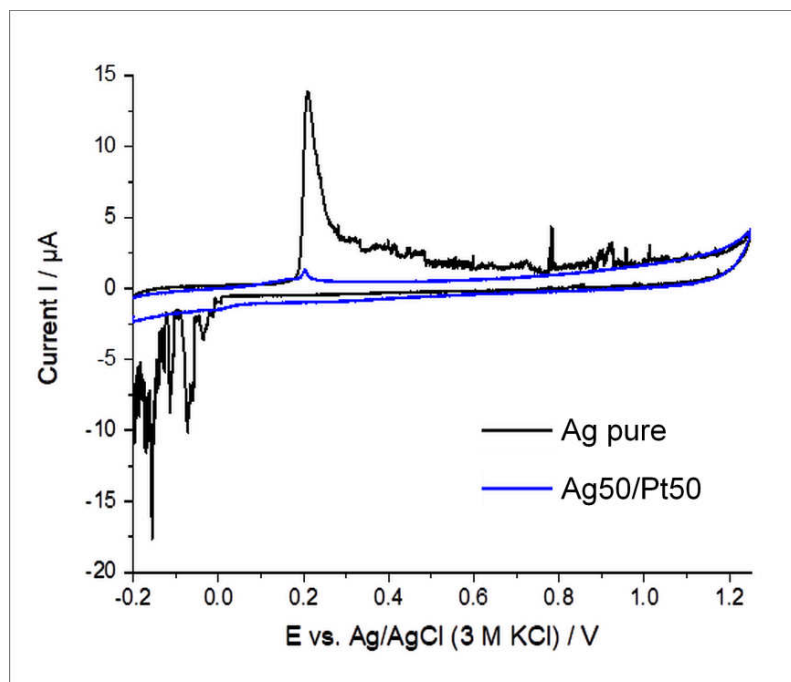


18 **Figure 4: Time-dependent UV-Vis absorption spectra of (A) pure Ag NP (50 μ g mL⁻¹)**
 19 **in RPMI and (B) the Ag50/Pt50 physical mixture (50 μ g mL⁻¹ of each NP) in RPMI.**
 20 **The peak at 400 nm corresponds to the surface plasmon resonance of Ag NP.**
 21

22
 23
 24 The Ag⁺ release within the Ag50/Pt50 physical mixture was investigated by CV
 25 analysis in comparison to pure Ag NP. The resulting cyclic voltammograms are
 26 shown in Figure 5.

1 Pure Ag NP displayed a large characteristic peak at about 0.2 V corresponding to the
 2 release of Ag^{I} due to Ag oxidation and associated to the formation of silver chloride
 3 in chloride-containing solvents (here 0.1 M HCl (aq)). The reduction of Ag^{I} to Ag
 4 occurred between 0.0 V and -0.2 V, which can be attributed to the reduction of the
 5 sparingly soluble silver chloride and is in accordance with published data [33,34]. For
 6 the physical NP mixture Ag50/Pt50 almost no signal for Ag oxidation and no Ag
 7 reduction signals were observed, which indicates an already completed Ag NP
 8 dissolution. Also no peak broadening and shifting to higher oxidation potentials (alloy
 9 signal) was observable, as reported for alloyed particles due to an electrochemical
 10 Ag stabilization [34,35].

11



12

13 **Figure 1:** Cyclic voltammograms of pure Ag NP and the physical mixture
 14 Ag50/Pt50. NP dispersions (1 mg mL^{-1}) were drop-cast onto the I E (2 r L pure Ag
 15 NP or 2 r L Ag NP and 2 r L Pt NP) and dried in an argon flow. CV measurements
 16 were performed in a 0.1 M HCl (aq) solution with a scan rate of 100 mV s^{-1} .

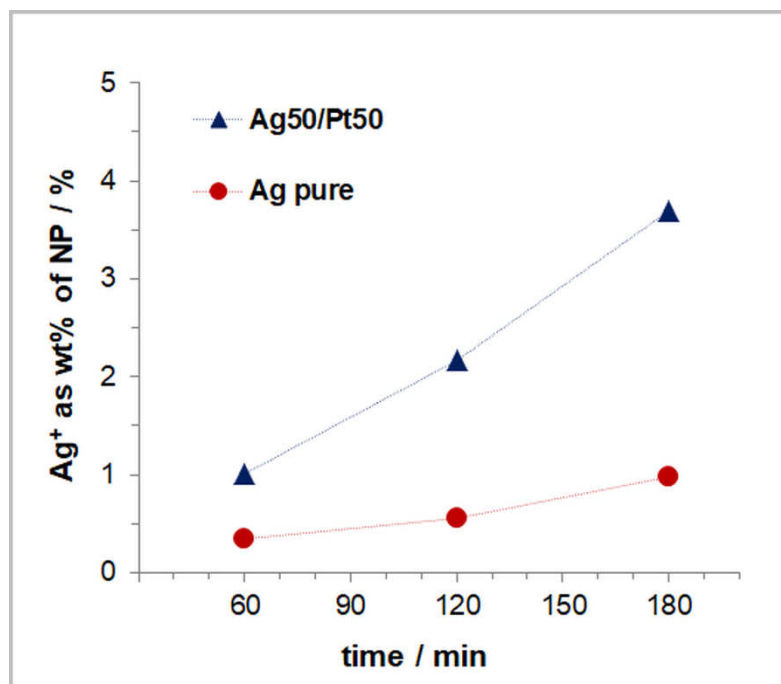
17

18 5.: \$,00(.7+(' \$ @ / * , = / ' +0\$

19 To prove whether the Ag^{I} release from Ag NP was enhanced in the presence of Pt
 20 NP in the physical mixture compared to pure Ag NP, dissolution experiments in cell
 21 culture medium RPMI were performed and the Ag^{I} release was analyzed by AAS.

1 As is shown in Figure 6, the amount of Ag^{I} released from pure Ag NP after 180 min
 2 of incubation was about 1 wt% of the total Ag NP mass. For the physical Ag50/Pt50
 3 mixture (containing same total Ag NP mass) 1 wt% Ag^{I} was released already after
 4 60 min of incubation and increased to 4 wt% Ag^{I} after 180 min of incubation
 5 (Figure 6). Hence, the quantity of released Ag^{I} from Ag NP was four times enhanced
 6 when Pt NP were present.

7



8

9 **Figure 6. Release of Ag^{I} as a function of time.** Pure Ag NP ($50 \text{ } \mu\text{g mL}^{-1}$) or a
 10 physical Ag50/Pt50 mixture ($50 \text{ } \mu\text{g mL}^{-1}$ of each NP) were incubated for 60 min,
 11 120 min and 180 min in RPMI. The released Ag^{I} was determined by AAS and is
 12 given as wt% of the total Ag NP mass applied.

13

14

15 $8 \times 10^8 \text{ CFU} / \text{mL}$, (

16

17 Here we have demonstrated that a higher Ag^{I} release due to a faster Ag NP
 18 dissolution occurred when Pt NP were mixed with Ag NP (physical mixture)
 19 compared to same amounts of pure Ag NP. This effect was obviously
 20 electrochemically driven by a sacrificial anode reaction, considering the applied cell
 21 biological and analytical examination (toxic effects on bacteria and hMSC, UV-Vis,
 22 CV, AAS).

1 The enhanced Ag⁺ release within the physical mixture was dependent on the ratio of
2 Ag NP and Pt NP. A significant increase in cytotoxic reactions of the physical
3 mixtures was observed with 50 wt% as well as 70 wt% Pt NP, while a Pt NP content
4 of 30 wt% was insufficient to provoke enhanced toxicity. To the best of our
5 knowledge, such a Pt-dependent enhancement of Ag dissolution has not yet been
6 described for NP mixtures. There are only few studies that have addressed biological
7 effects of sacrificial anode-like systems consisting of Ag and Pt. Dowling et al. [18] and
8 Jiang et al. [19] demonstrated increased antimicrobial activity of bimetallic AgPt coatings
9 compared to pure Ag due to an enhanced Ag⁺ release [18,19]. The utilization of Ag
10 dot arrays on Pt thin films as a sacrificial anode system was previously reported by
11 our group and its efficiency to combat adherent and planktonic bacteria was
12 confirmed [13].

13 Time-lapse microscopy and dissolution experiments demonstrated a fast Ag⁺ release
14 within the physical mixture. This is probably the reason for the electrochemical results
15 obtained by cyclic voltammetry. The cyclic voltammogram recorded for the physical
16 mixture showed an already completed Ag⁺ release (no Ag oxidation and no Ag
17 reduction signals) in contrast to the behavior of pure Ag NP, obviously due to the
18 experimental setup, which required a droplet-drying phase before measurement.

19 Recently, we reported that bimetallic AgPt NP with an alloy-like structure (diameter
20 about 10 nm) did not show any sacrificial anode effect for Ag [20,21], which is
21 apparently a consequence of an increase in the redox potential of Ag in a Pt alloy.
22 Such an electrochemical stabilization of Ag was also described for bimetallic alloyed
23 AgAu NP [34–36]. The absence of a sacrificial anode effect in alloyed systems
24 suggests that a sufficient physical separation of the metals is necessary to induce
25 sacrificial anode effects. For most practical applications of sacrificial anode systems
26 (e.g. corrosion protection), there is such a physical separation of the bulk material, but
27 the materials are in electrical contact [15]. A physical NP mixture is different in terms
28 of the contact between the metals. A NP within a physical mixture interacts with
29 others by collision due to random motion of the NP in suspension (convection and
30 Brownian motion). The fact that the plasmon resonance of the Ag NP rapidly
31 decreased in the presence of Pt NP suggests that the interaction of both particle
32 types led to a morphological alteration of the Ag NP [26,30,31,37].

33 As was reported by Toshima et al. [16] and Hirakawa et al. [16] physical mixtures of Ag NP
34 (diameter about 10 nm) and more noble metal NP (platinum, palladium, rhodium;

1 diameter 2 - 3 nm) led to a spontaneous formation of bimetallic core/shell structured
2 NP, consisting of an Ag core with a shell of the more noble metal [32,38–42]. They
3 also observed a fast decline of the Ag plasmon peak in the respective physical
4 mixtures, which was related to the coverage of the Ag NP surface with the more
5 noble NP. Although the authors did not consider the electrochemical dissolution of Ag
6 NP, they reported that the emerging bimetallic NP were smaller than the original Ag
7 NP, which suggests that at least a partial dissolution of Ag NP occurred.

8 Currently, we cannot exclude that such a clustering of Ag NP and Pt NP occurred in
9 our experimental physical mixtures, therefore the detailed mechanism of Ag⁺ release
10 enhancement within the studied physical mixtures still needs to be investigated in
11 detail. Nevertheless, we suggest an underlying sacrificial anode mechanism which
12 results in an enhanced Ag⁺ release.

13 Very recently we reported that small Pt NP (as used in this study) exhibit an osteo-
14 promotive activity on hMSC [21]. Therefore, physical mixtures of Ag NP and Pt NP
15 could be useful for the development of novel biomaterials with enhanced
16 antimicrobial activity and osteo-supportive properties at a reduced silver content,
17 thereby reducing the inherent toxicity to the surrounding tissue.

18
19

1 93' 4%&\$0 , #(- :(0 \$3%#\$(

2 None.

3

4

5 ! ' ; , - < 4B. =3> 3, \$

6 Supported by the Deutsche Forschungsgemeinschaft (DFG) in the projects EP
7 22/44-1, SE 2449/2-1, and HE 7192/2-1. I e thank Kerstin Brauner and Robin Meya
8 for AAS measurements.

9

1 73:3%, ' 3#(

2

- 3 [1] C.L. Roman{ , M. Toscano, D. Roman{ , L. Drago, Antibiofilm agents and implant-
4 related infections in orthopaedics: I here are we| J. Chemother. 25 (2) (2013)
5 67–80. <https://doi.org/10.1179/1973947812}.0000000045>.
- 6 [2] V. Alt, T. Bechert, P. Steinrücke, M. I agener, P. Seidel, E. Dingeldein, E.
7 Domann, R. Schnettler, An in vitro assessment of the antibacterial properties and
8 cytotoxicity of nanoparticulate silver bone cement, *Biomaterials* 25 (18) (2004)
9 4383–4391. <https://doi.org/10.1016/zbiomaterials.2003.10.078>.
- 10 [3] B. Nowack, H.F. Krug, M. Height, 120 years of nanosilver history: Implications for
11 policy makers, *Environ. Sci. Technol.* 45 (4) (2011) 1177–1183.
12 <https://doi.org/10.1021/es103316m>
- 13 [4] ~.L. Feng, J. I u, G.~ . Chen, F.j . Cui, T.N. Kim, J.k . Kim, A mechanistic study
14 of the antibacterial effect of silver ions on *Escherichia coli* and *Staphylococcus*
15 *aureus*, *J. Biomed. Mater. Res.* 52 (4) (2000) 662–668.
16 [https://doi.org/10.1002/1097-4636\(20001215\)52:4 662:AID-JBM10n3.0.Ck ;2-3](https://doi.org/10.1002/1097-4636(20001215)52:4 662:AID-JBM10n3.0.Ck ;2-3).
- 17 [5] C.H. Ho, E.K. k dermat, I. Berndt, J.C. Tiller, Long-term active antimicrobial
18 coatings for surgical sutures based on silver nanoparticles and hyperbranched
19 polylysine, *J. Biomater. Sci. Polym. Ed.* 24 (13) (2013) 1589–1600.
20 <https://doi.org/10.1080/09205063.2013.782803>.
- 21 [6] M.H. Kollef, B. Afessa, A. Anzueto, C. Veremakis, K.M. Kerr, B.D. Margolis, D.E.
22 Craven, P.R. Roberts, A.C. Arroliga, R.D. Hubmayr, M.I. Restrepo, I .R. Auger,
23 R. Schinner, Silver-coated endotracheal tubes and incidence of ventilator-
24 associated pneumonia: The NASCENT randomized trial, *JAMA* 300 (7) (2008)
25 805–813. <https://doi.org/10.1001/zama.300.7.805>.
- 26 [7] R. Vazmuez-Mu oz, B. Borrego, K. Ju rez-Moreno, M. Garc a-Garc a, J.D. Mota
27 Morales, N. Bogdanchikova, A. Huerta-Samuero, Toxicity of silver nanoparticles
28 in biological systems: Does the complexity of biological systems matter| *Toxicol.*
29 *Lett.* 276 (2017) 11–20. <https://doi.org/10.1016/ztoxlet.2017.05.007>.
- 30 [8] S. Ahlberg, A. Antonopulos, J. Diendorf, R. Dringen, M. Epple, R. Flöck, I .
31 Goedecke, C. Graf, N. Haberl, J. Helmlinger, F. Herzog, F. Heuer, S. Hirn, C.
32 Johannes, S. Kittler, M. Köller, K. Korn, I .G. Kreyling, F. Krombach, J.
33 Lademann, K. Loza, E.M. Luther, M. Malissek, M.C. Meinke, D. Nordmeyer, A.
34 Pailliant, J. Raabe, F. Rancan, B. Rothen-Rutishauser, E. Rühl, C. Schleh, A.

- 1 Seibel, C. Sengstock, L. Treuel, A. Vogt, K. I eber, R. j ellner, PVP-coated,
2 negatively charged silver nanoparticles: A multi-center study of their
3 physicochemical characteristics, cell culture and in vivo experiments, *Beilstein J.*
4 *Nanotechnol.* 5 (2014) 1944–1965. <https://doi.org/10.3762/bnano.5.205>.
- 5 [9] M. Ahamed, M. Karns, M. Goodson, J. Rowe, S.M. Hussain, J.J. Schlager, } .
6 Hong, DNA damage response to different surface chemistry of silver
7 nanoparticles in mammalian cells, *Toxicol. Appl. Pharmacol.* 233 (3) (2008) 404–
8 410. <https://doi.org/10.1016/ztaap.2008.09.015>.
- 9 [10] K. Loza, J. Diendorf, C. Sengstock, L. Ruiz-Gonzalez, J.M. Gonzalez-Calbet, M.
10 Vallet-Regi, M. Köller, M. Epple, The dissolution and biological effects of silver
11 nanoparticles in biological media, *J. Mater. Chem. B* 2 (12) (2014) 1634.
12 <https://doi.org/10.1039/c3tb21569e>.
- 13 [11] S. Chernousova, M. Epple, Silver as antibacterial agent: Ion, nanoparticle, and
14 metal, *Angew. Chem. Int. Ed Engl.* 52 (6) (2013) 1636–1653.
15 <https://doi.org/10.1002/anie.201205923>.
- 16 [12] M. Köller, C. Sengstock, } . Motemani, C. Khare, P.J.S. Buenconsejo, J. Geukes,
17 T.A. Schildhauer, A. Ludwig, Antibacterial activity of microstructured Ag/Au
18 sacrificial anode thin films, *Mater. Sci. Eng. C Mater. Biol. Appl.* 46 (2015) 276–
19 280. <https://doi.org/10.1016/zmsec.2014.10.058>.
- 20 [13] M. Köller, P. Bellova, S.M. Javid, } . Motemani, C. Khare, C. Sengstock, K.
21 Tschulik, T.A. Schildhauer, A. Ludwig, Antibacterial activity of microstructured
22 sacrificial anode thin films by combination of silver with platinum group elements
23 (platinum, palladium, iridium), *Mater. Sci. Eng. C Mater. Biol. Appl.* 74 (2017)
24 536–541. <https://doi.org/10.1016/zmsec.2016.12.075>.
- 25 [14] A. Abuayyash, N. j iegler, J. Gessmann, C. Sengstock, T.A. Schildhauer, A.
26 Ludwig, M. Köller, Antibacterial Efficacy of Sacrificial Anode Thin Films
27 Combining Silver with Platinum Group Elements within a Bacteria-Containing
28 Human Plasma Clot, *Adv. Eng. Mater.* 20 (2) (2018) 1700493.
29 <https://doi.org/10.1002/adem.201700493>.
- 30 [15] S. Szabo, I. Bakos, Cathodic Protection with Sacrificial Anodes, *Corrosion*
31 *Reviews* 24 (3-4) (2006) 18. <https://doi.org/10.1515/Ck RRREV.2006.24.3-4.231>.
- 32 [16] G.J. Bruce, D.J. Eyres (Eds.), *Ship Construction*, 7th ed., Elsevier; Butterworth-
33 Heinemann, Amsterdam, kxford, 2012.

- 1 [17] J. Chaussard, J.-C. Folest, J.-} . Nedelec, J. Perichon, S. Sibille, M. Troupel, Use
2 of Sacrificial Anodes in Electrochemical Functionalization of k rganic Halides,
3 Synthesis 1990 (05) (1990) 369–381. <https://doi.org/10.1055/s-1990-26880>.
- 4 [18] M. j hang, } . j hao, L. } an, R. Peltier, l . Hui, u. } ao, } . Cui, u. Chen, H. Sun,
5 j . l ang, Interfacial Engineering of Bimetallic Ag/Pt Nanoparticles on Reduced
6 Graphene k xide Matrix for Enhanced Antimicrobial Activity, ACS Appl. Mater.
7 Interfaces 8 (13) (2016) 8834–8840. <https://doi.org/10.1021/acsami.6b01396>.
- 8 [19] D.P. Dowling, A.J. Betts, C. Pope, M.L. McConnell, R. Eloy, M.N. Arnaud, Anti-
9 bacterial silver coatings exhibiting enhanced activity through the addition of
10 platinum, Surface and Coatings Technology 163-164 (2003) 637–640.
11 [https://doi.org/10.1016/S0257-8972\(02\)00689-8](https://doi.org/10.1016/S0257-8972(02)00689-8).
- 12 [20] V. Grasmik, M. Breisch, K. Loza, M. Heggen, M. Köller, C. Sengstock, M. Epple,
13 Synthesis and biological characterization of alloyed silver–platinum
14 nanoparticles: From compact core–shell nanoparticles to hollow nanoalloys, RSC
15 Adv. 8 (67) (2018) 38582–38590. <https://doi.org/10.1039/C8RA06461J>.
- 16 [21] M. Breisch, V. Grasmik, K. Loza, K. Pappert, A. Rostek, N. j iegler, A. Ludwig, M.
17 Heggen, M. Epple, J.C. Tiller, T.A. Schildhauer, M. Köller, C. Sengstock,
18 Bimetallic silver-platinum nanoparticles with combined osteo-promotive and
19 antimicrobial activity, Nanotechnology 30 (30) (2019) 305101.
20 <https://doi.org/10.1088/1361-6528/ab172b>.
- 21 [22] A. Rostek, M. Breisch, K. Pappert, K. Loza, M. Heggen, M. Köller, C. Sengstock,
22 M. Epple, Comparative biological effects of spherical noble metal nanoparticles
23 (Rh, Pd, Ag, Pt, Au) with 4–8 nm diameter, Beilstein J. Nanotechnol. 9 (2018)
24 2763–2774. <https://doi.org/10.3762/bnano.9.258>.
- 25 [23] I. Brook, Inoculum Effect, Clinical Infectious Diseases 11 (3) (1989) 361–368.
26 <https://doi.org/10.1093/clinids/11.3.361>.
- 27 [24] C. Tan, R.P. Smith, J.K. Srimani, K.A. Riccione, S. Prasada, M. Kuehn, L. } ou,
28 The inoculum effect and band-pass bacterial response to periodic antibiotic
29 treatment, Mol. Syst. Biol. 8 (2012) 617. <https://doi.org/10.1038/msb.2012.49>.
- 30 [25] C. Greulich, D. Braun, A. Peetsch, J. Diendorf, B. Siebers, M. Epple, M. Köller,
31 The toxic effect of silver ions and silver nanoparticles towards bacteria and
32 human cells occurs in the same concentration range, RSC Adv. 2 (17) (2012)
33 6981. <https://doi.org/10.1039/c2ra20684f>.

- 1 [26] S. Agnihotri, S. Mukherz, S. Mukherz, Size-controlled silver nanoparticles
2 synthesized over the range 5–100 nm using the same protocol and their
3 antibacterial efficacy, *RSC Adv.* 4 (8) (2014) 3974–3983.
4 <https://doi.org/10.1039/C3RA44507K>.
- 5 [27] C. Noguez, Surface Plasmons on Metal Nanoparticles: The Influence of Shape
6 and Physical Environment, *J. Phys. Chem. C* 111 (10) (2007) 3806–3819.
7 <https://doi.org/10.1021/ϕ066539m>.
- 8 [28] A.L. Gonzalez, C. Noguez, Influence of Morphology on the Optical Properties of
9 Metal Nanoparticles, *Jnl of Comp Theo Nano* 4 (2) (2007) 231–238.
10 <https://doi.org/10.1166/ztn.2007.2309>.
- 11 [29] C. Chapon, M.F. Gillet, C.R. Henry (Eds.), *Small Particles and Inorganic
12 Clusters: Proceedings of the Fourth International Meeting on Small Particles and
13 Inorganic Clusters University Aix-Marseille III Aix-en-Provence, France, 5-9 July
14 1988*, Springer Berlin Heidelberg, Berlin, Heidelberg, 1989.
- 15 [30] R. Desai, V. Mankad, S. Gupta, P. Jha, Size Distribution of Silver Nanoparticles:
16 UV-Visible Spectroscopic Assessment, *nanosci nanotechnol lett* 4 (1) (2012) 30–
17 34. <https://doi.org/10.1166/nnl.2012.1278>.
- 18 [31] G. Mie, Contributions to the optics of turbid media particularly of colloidal metal
19 solutions, *Ann. Phys.* 330 (3) (1908) 377–445.
20 <https://doi.org/10.1002/andp.19083300302>.
- 21 [32] N. Toshima, M. Kanemaru, } . Shiraishi, } . Koga, Spontaneous formation of
22 core/shell bimetallic nanoparticles: A calorimetric study, *J. Phys. Chem. B* 109
23 (34) (2005) 16326–16331. <https://doi.org/10.1021/ϕ051400h>.
- 24 [33] H.S. Toh, C. Batchelor-McAuley, K. Tschulik, R.G. Compton, Electrochemical
25 detection of chloride levels in sweat using silver nanoparticles: A basis for the
26 preliminary screening for cystic fibrosis, *Analyst* 138 (15) (2013) 4292–4297.
27 <https://doi.org/10.1039/C3AN00843F>.
- 28 [34] E.N. Saw, V. Grasmik, C. Rurainsky, M. Epple, K. Tschulik, Electrochemistry at
29 single bimetallic nanoparticles - using nano impacts for sizing and compositional
30 analysis of individual AgAu alloy nanoparticles, *Faraday Discuss.* 193 (2016)
31 327–338. <https://doi.org/10.1039/c6fd00112b>.
- 32 [35] N. Alissawi, V. japorozhenko, T. Strunskus, I. Kocabas, V.S.K.
33 Chakravadhanula, L. Kienle, D. Garbe-Schönberg, F. Faupel, Effect of gold
34 alloying on stability of silver nanoparticles and control of silver ion release from

- 1 vapor-deposited Ag–Au/polytetrafluoroethylene nanocomposites, *Gold Bull* 46
2 (1) (2013) 3–11. <https://doi.org/10.1007/s13404-012-0073-6>.
- 3 [36] V. Grasmik, C. Rurainsky, K. Loza, M.V. Evers, k. Prymak, M. Heggen, K.
4 Tschulik, M. Epple, Deciphering the Surface Composition and the Internal
5 Structure of Alloyed Silver-Gold Nanoparticles, *Chemistry* 24 (36) (2018) 9051–
6 9060. <https://doi.org/10.1002/chem.201800579>.
- 7 [37] S.M. k za, } . Fan, C.M. Armstrong, P. Defnet, B. j hang, *Nanoscale*
8 *Electrochemistry Revisited*, *Anal. Chem.* 88 (1) (2016) 414–430.
9 <https://doi.org/10.1021/acs.analchem.5b04542>.
- 10 [38] K. Hirakawa, Self-k rganization of Silver-Core Bimetallic Nanoparticles and Their
11 Application for Catalytic Reaction, in: A.A. Hashim (Ed.), *Smart nanoparticles*
12 *technology*, InTech, Rižeka, Croatia, 2012. <https://doi.org/10.5772/33918>
- 13 [39] K. Hirakawa, N. Toshima, Ag/Rh Bimetallic Nanoparticles Formed by Self-
14 assembly from Ag and Rh Monometallic Nanoparticles in Solution, *Chem. Lett.*
15 32 (1) (2003) 78–79. <https://doi.org/10.1246/cl.2003.78>.
- 16 [40] T. Matsushita, } . Shiraishi, S. Horiuchi, N. Toshima, Synthesis and Catalysis of
17 Polymer-Protected Pd/Ag/Rh Trimetallic Nanoparticles with a Core–Shell
18 Structure, *BCSJ* 80 (6) (2007) 1217–1225. <https://doi.org/10.1246/bcsz80.1217>.
- 19 [41] N. Toshima, Capped Bimetallic and Trimetallic Nanoparticles for Catalysis and
20 Information Technology, *Macromol. Symp.* 270 (1) (2008) 27–39.
21 <https://doi.org/10.1002/masy.200851004>.
- 22 [42] K. Hirakawa, T. Kaneko, N. Toshima, Kinetics of Spontaneous Bimetallization
23 between Silver and Noble Metal Nanoparticles, *Chemistry – An Asian Journal* 13
24 (15) (2018) 1892–1896. <https://doi.org/10.1002/asia.201800633>.

25